Journal of Magnetic Resonance 300 (2019) 149–152

Contents lists available at ScienceDirect

Journal of Magnetic Resonance

journal homepage: www.elsevier.com/locate/jmr

In-situ Overhauser-enhanced nuclear magnetic resonance at less than 1 μT using an atomic magnetometer

Hyun Joon Lee [a,b], Seong-Joo Lee [a], Jeong Hyun Shim [a], Han Seb Moon [b], Kiwoong Kim [a,*]

[a] Ultra-low Magnetic Field Team, Korea Research Institute of Standards and Science (KRISS), 267, Gajeong-ro, Yuseong-gu, Daejeon 34113, Republic of Korea
[b] Department of Physics, Pusan National University, 2, Busandaehak-ro 63beon-gil, Geumjeong-gu, Busan 46241, Republic of Korea

ARTICLE INFO

Article history:
Received 20 September 2018
Revised 16 January 2019
Accepted 8 February 2019
Available online 10 February 2019

Keywords:
Dynamic nuclear polarization
Atomic magnetometer
Ultralow-field NMR

ABSTRACT

The development of atomic magnetometers has led to nuclear magnetic resonance (NMR) in zero and ultralow magnetic fields without using cryogenic sensors. However, *in-situ* detection, meaning that a sample locates in the detection space beside a vapor cell, has been conducted only with parahydrogen-induced polarization. Other hyperpolarization techniques remain unexplored yet. In this work, we demonstrate that Overhauser dynamic nuclear polarization allows *in-situ* NMR detection with an atomic magnetometer at less than 1 μT. The ^{1}H NMR signal of a nitroxide radical solution was observed at 13.83 Hz, which corresponds to 325 nT. Signal-to-noise ratio was 32 after sixteen averages. On the Larmor precession of ^{1}H spins, a decaying oscillation was superimposed. We attribute it to a transient ^{87}Rb spin precession in response to a non-adiabatic field variation. This work shows a new capability of zero- and ultralow-field NMR.

1. Introduction

Nuclear magnetic resonance (NMR) is generally performed in high magnetic fields to increase chemical shift resolution and to maximize detection sensitivity by enhancing thermal polarization. For this reason, commercial NMR and magnetic resonance imaging (MRI) instrumentation has focused on increasing the main magnetic fields of the systems. The poor magnetic sensitivity of *rf* coil-based NMR detectors in low magnetic fields, however, has been an obstacle to many possible applications at low frequencies ranging from DC to below 1 kHz [1–4]. The first detection system which utilized a superconducting quantum interferometer (SQUID) [5,6], was able to directly detect NMR signals in the zero field and was leading sensor for a long time. Unfortunately, SQUIDs require helium cryogenics, which required costly maintenance.

In recent years, atomic magnetometers (AMs) have proven to be competitive with SQUIDs in terms of sensitivity, without the need for cryogenic operation. To date, several NMR/MRI studies based on AMs have been reported [7–17]. Savukov et al. performed NMR detection using a flow system such that the sample is prepolarized using a permanent magnet outside of the shields to avoid the magnetization of magnetic shields [12–14]. Liu et al. detected NMR signals using a shuttle system whereby samples were prepolarized using a permanent magnet outside the magnetic shields, and pneumatically shuttled into the detection region [10]. The use of AMs facilitates an acceptable signal-to-noise ratio (SNR) with single-shot NMR sampling due to their high sensitivity in the low frequency range. However, these remote detection schemes require strong permanent magnets which complicates the experimental setup. In addition, a broadened NMR spectral linewidth was observed in these systems due to the dispersion of water while flowing in the tube. Even if a permanent magnet was not used, a pre-polarization field (B_p), electrically switched on and off, must be applied to magnetize the sample before acquisition. A strong B_p cause side effects such as eddy current induction in the magnetic shielding wall, which broadens the NMR linewidth and has an adverse effect on NMR measurements [18,19].

Recently, there has been growing interest in the high efficiency of dynamic nuclear polarization (DNP) that boosts signal intensity in NMR experiments by transferring spin polarization from electrons to nuclei via cross-relaxation. DNP-NMR provides an alternative approach to measurement techniques with inherently poor sensitivity at low magnetic fields down to sub-millitesla [20–24].

In this work, we take advantage of the fact that as the magnetic field approaches zero, the difference between the resonance frequency of the Rb atom and the nucleus becomes smaller. However, at room temperature, the polarization of protons is too small to be measured, so we use DNP, which can be classified as a hyperpolarization method. DNP-NMR makes it possible to transfer the Boltz-

* Corresponding author.
E-mail address: kwkim@kriss.re.kr (K. Kim).

https://doi.org/10.1016/j.jmr.2019.02.001
1090-7807/© 2019 The Authors. Published by Elsevier Inc.

mann polarization of the electron spin to the nuclear spin, thus providing a boost in the NMR signal intensity by several orders of magnitude. Many studies on DNP measurement using SQUID have been reported [25–28], but to the best of our knowledge, there are no reported studies based on AMs. Herein, we demonstrate the *in-situ* detection of NMR signals from a water sample using an AM by utilizing spin-exchange relaxation free (SERF) regime, which achieves a noise level of 20 $\mathrm{fT/Hz^{1/2}}$ at 10 Hz. Signals with a SNR of about 32 and a spectral width of 0.7 Hz were obtained in a 2 mM TEMPOL solution.

2. Methods

Fig. 1(a) shows an experimental setup for *in-situ* measurements of ultralow magnetic fields (ULF)-NMR. To avoid the effects of external magnetic noise, the equipment for ULF-NMR experiments was installed inside a specially designed magnetically shielded room [3]. The equipment includes two major parts: One is the AM which serves as the magnetic sensor for NMR detection. The other part is the ULF-DNP's magnetic field generation system consisting of a Helmholtz coil, solenoid coil, and circular coil.

A commercial SERF cm-scale AM (QZFM, QuSpin) was employed as the NMR signal detector based on zero-field resonance with a single laser beam. The measured noise level was less than 20 $\mathrm{fT/Hz^{1/2}}$ in the range from 1 to 150 Hz. This atomic magnetometer is primarily sensitive to a static or slowly varying magnetic field, more specifically, to the $\hat{y}$-component of the magnetic field. In the presence of a ULF along the $\hat{z}$ direction, the Larmor precession of spins in the sample produces a low-frequency signal from several hertz to a few hundred hertz, corresponding to alternating magnetic field, whose projection in the $\hat{y}$ direction can be monitored using the atomic magnetometer.

B_p and the measurement field (B_m) were generated using the Helmholtz coil and the solenoid coil, respectively. The Helmholtz coil generates a magnetic field of 58 μT in the axial direction, with an inhomogeneity of about 3% within 50 mm of the coil's center. The length of the solenoid coil was set to 130 mm in order to minimize the influence of B_m on the atomic magnetometer. The B_m strength was about 325 nT, which corresponds to the NMR frequency, $\omega_m = \gamma_p B_m \approx 13.83$ Hz, where γ_p is proton's gyromagnetic ratio. We generated *rf* field (B_{rf}) using a circular coil to increase the *rf* power efficiency for saturation of the ESR transition.

The *rf* resonance circuit is shown in Fig. 1(b). It has a tuning range from 65 MHz to 125 MHz and a target frequency of 74.4 MHz. The directions of B_{rf}, and B_p were perpendicular to each other where only π transitions will occur [22]. Taking into account the skin depth of the copper windings, the coils should be designed so that not only does B_{rf} reach the sample, but B_m has a minimal effect on the magnetometer. Since *in-situ* detection is utilized, there is no significant signal loss due to T_1 during the experiment, as well as the ability to quickly measure multiple samples.

We used commercially available 4-Hydroxy-2,2,6,6-tetramethyl piperidine-1-oxyl (TEMPOL; Sigma-Aldrich), which has an unpaired electron. 2 mM of TEMPOL solution was prepared with deionized water and placed inside the solenoid coil.

The timing sequence for the ULF-DNP experiment was the same as in Ref. [27]. (More detailed description can be found in the Supplementary Material.) For the pre-polarization, we apply B_p in the $\hat{x}$ direction and simultaneously apply B_{rf} in the $\hat{z}$ direction during the polarization period to cause the electron spin of the TEMPOL radical to saturation. After these fields are turned off, the NMR signal is detected while applying B_m during measurement time. The free induction decay (FID) signals were averaged after sixteen measurements with and without B_{rf}, respectively, and were Fourier transformed with FID time traces.

3. Results and discussion

Fig. 2(a) and (d) presents the NMR and FFT signal, respectively, when B_{rf} is turned off. As shown in the figure, when B_p is as low as 58 μT (Boltzmann distribution $\approx 10^{-6}$ at room temperature), the NMR signal is not observed at the resonance frequency ω_m. Instead, we can observe an exponentially decaying signal which oscillates at 5.45 Hz. Generally, the transverse relaxation time of the Rb spins is much shorter than that of the protons in water, so the transient signal of the magnetometer decays faster than the water spin-precession signal. However, the behavior of the magnetometer is different when B_{rf} and B_p, which is far beyond the dynamic range (±5 nT) of the magnetometer, is applied. The behavior of the atomic spin is described phenomenologically by the Bloch equation and we can express a steady state solution with optical pumping rate (align the spin direction along the pumping axis), total relaxation rate (randomize the spin direction) and an ambient magnetic field (induces the spin to precess in the plane

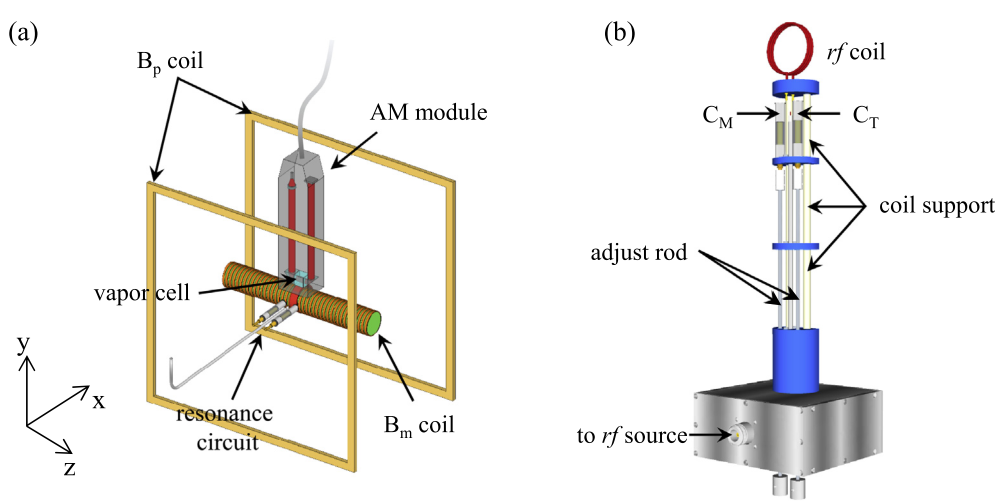

Fig. 1. (a) Schematic of the ULF-DNP experimental setup. The directions of B_m and B_{rf} are parallel, and these of B_{rf} and B_p are perpendicular to each other. The sample was contained in a bottle with an outer diameter of 27 mm and a length of 70 mm and was centered inside of the solenoid coil surrounded by an *rf* coil. The AM's 3 × 3 × 3 mm³ Rb vapor cell is located approximately 12 mm away from the center of the sample. (b) The diagram of the circular-coil and resonance circuit used to generate a *rf* field. C_M is the matching capacitor (0.8–38 pF), and C_T is the tuning capacitor (2–120 pF). All components include coil support and the adjust rods are made from non-magnetic materials.

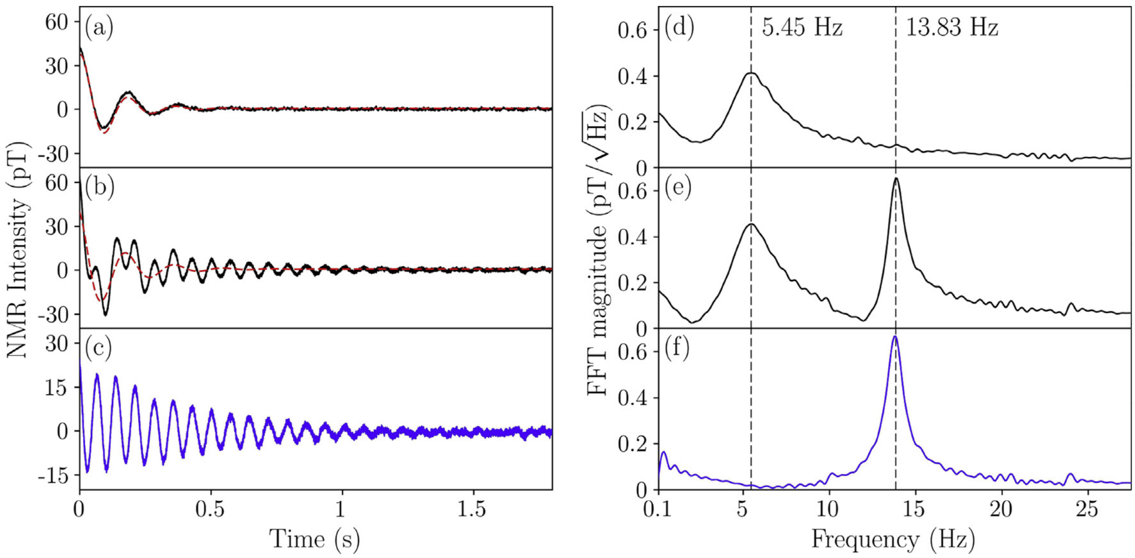

Fig. 2. The *in-situ* DNP measurement for an average of 16 samples and its FFT spectra. (a) The background signal without B_{rf}. The signal oscillates at a specific frequency, which can be described in terms of the Larmor frequency of the Rb atoms and spin–spin exchange relaxation (red dashed line). (b) The DNP-NMR signal with B_{rf}. The Dashed line shows a fitting curve of the DNP-NMR signal with Eq. (1) from which the value of T_2^* and the residual field were determined to be 130 ms and 0.8 nT, respectively. (c) The pure NMR signal was obtained by signal processing which entailed subtracting the fitting value from the experimental results. (d), (e), (f) The FFT spectra corresponding to the signals shown in (a), (b), and (c), respectively. The unprocessed raw data is in the Supplementary Material.

perpendicular to the field) [29]. The net direction of the atomic spin vector is determined by the competition between those three parameters, in our experiment the strong ambient field is dominant in atomic spin direction. When B_{rf} and B_p were turned off, the Rb atoms return to the polarized state satisfying SERF condition with a narrow magnetic linewidth. As in the SERF regime, a sufficiently low relaxation rate (within a few hundred ms), the AM's polarization will exhibit oscillations at its natural frequencies due to the residual magnetic field. This occurs at the Zeeman resonance frequency (Larmor frequency) of the Rb atoms. Thus, switching off B_{rf} reveals oscillations at the Larmor frequency. The red dashed line in Fig. 2(a) represents the calculated solution for the $\hat{x}$-component (direction of the pump beam) of the polarization. The solution is expressed with the oscillating frequency ω and the relaxation time T_2^* as follows: [30]

$$S_x(t) = S_{0x}\sin(\omega t + \Phi)e^{-\frac{t}{T_2^*}} + O, \tag{1}$$

in which S_{0x} is the steady-state value of $S_x(t), \Phi$ is the phase angle and O is the offset. The oscillating frequency $\omega = \gamma\mathbf{B}$ is the Larmor frequency of the ^{87}Rb atoms with a gyromagnetic ratio of γ = 7 Hz/nT under the influence of the residual magnetic field **B**. From Fig. 2(a), it determined that the AM has a T_2^* of 110 ms and the residual magnetic field near the AM is about 0.8 nT.

Fig. 2(b) and (e) shows the DNP-NMR and FFT magnitude measured with B_{rf}. We obtained an enhanced NMR signal at 13.83 Hz via the saturation of a selective excitation of electrons of nitroxide radicals. Based on the good agreement of the fitting results in Fig. 2(a), the background oscillation of the signal was fitted as shown in Fig. 2(b). In order to investigate the pure DNP-NMR signal while excluding the effect of the residual magnetic field, we subtracted the fitting result from the raw signal as shown in Fig. 2(c). The signal, measured in 30 cc of a 2 mM TEMPOL solution, is due to an *in-situ* hyperpolarized nuclear spin.

Fig. 2(f) shows the FFT of the NMR signal shown in Fig. 2(c). Its SNR is approximately 32, which was calculated by the signal amplitude divided by the root mean square of the noise amplitude at the frequency range between 30 and 40 Hz. (The experimental results and SNR value obtained by shifting the NMR frequency higher than 13.83 Hz to avoid the influence of Rb oscillatory magnetic field are in the Supplementary Material.) The value of T_2^* from Fig. 2(c) is approximately 450 ms and exhibits a linewidth of approximately 0.71 Hz. Considering that T_2 is typically 2.6 s (linewidth is 0.12 Hz) for water, a linewidth expansion of approximately 0.6 Hz was observed. This can be explained by an inhomogeneous B_m in the sample area, which corresponds to ΔB = 9 nT.

4. Conclusions

In this work, we experimentally demonstrated *in-situ* measurement of an enhanced ^{1}H NMR signals of water in 2 mM TEMPOL solution using an atomic magnetometer. From our results, *in-situ* measurements were shown to drastically reduce the single sampling time to obtain AM-based NMR signals, and this is advantageous for acquiring averaged signals. This is expected to directly facilitate the measurement of rapidly changing signals and sample of low molar concentration. Since AMs provide an alternative approach to low field NMR due to their intrinsic sensitivity at low frequencies, the experimental results are promising for potential application to hyperpolarization with AMs for ultralow field NMR and MRI without the limitations imposed by high magnetic field requirements.

Acknowledgments

This work was supported by a Development of Next-generation Measurement Technology for Biomagnetic Resonance (GP2018-0021) grant and Development of Platform Technology for Innovative Medical Measurements Program (GP2019-0013) grant from the Korea Research Institute of Standards and Science.

Appendix A. Supplementary material

Supplementary data associated with this article can be found, in the online version, at https://doi.org/10.1016/j.jmr.2019.02.001.

References

[1] S.K. Lee, M. Mößle, W. Myers, N. Kelso, A.H. Trabesinger, A. Pines, J. Clarke, SQUID-detected MRI at 132 μT with T_1-weighted contrast established at 10 μT-300 mT, Magn. Reson. Med. 53 (2004) 9–14.
[2] S. Busch, M. Hatridge, M. Mößle, W. Myers, T. Wong, M. Mück, K. Chew, K. Kuchinsky, J. Simko, J. Clarke, Measurements of T_1-relaxation in ex vivo prostate tissue at 132 μT, Magn. Reson. Med. 67 (2012) 1138–1145.
[3] K. Kim, S.-J. Lee, C.S. Kang, S.-m. Hwang, Y.-H. Lee, K.-K. Yu, Toward a brain functional connectivity mapping modality by simultaneous imaging of coherent brainwaves, NeuroImage 91 (2014) 63–69.
[4] S.-J. Lee, J.H. Shim, K. Kim, S.-m. Hwang, K.-K. Yu, S. Lim, J.H. Han, H. Yim, J.-H. Kim, Y.S. Jung, K.S. Kim, T_1 relaxation measurement of ex-vivo breast cancer tissues at ultralow magnetic fields, Biomed. Res. Int. 2015 (2015) 385428.
[5] R. McDermott, A.H. Trabesinger, M. Mück, E.L. Hahn, A. Pines, J. Clarke, Liquid-state NMR and scalar couplings in microtesla magnetic fields, Science 295 (2002) 2247–2249.
[6] A.H. Trabesinger, R. McDermott, S. Lee, M. Mück, J. Clarke, A. Pines, SQUID-detected liquid state NMR in microtesla fields, J. Phys. Chem. A 108 (2004) 957–963.
[7] M.P. Ledbetter, S. Pustelny, D. Budker, M.V. Romalis, J.W. Blanchard, A. Pines, Liquid-state nuclear spin comagnetometers, Phys. Rev. Lett. 108 (2012) 243001.
[8] P.J. Ganssle, H.D. Shin, S.J. Seltzer, V.S. Bajaj, M.P. Ledbetter, D. Budker, S. Knappe, J. Kitching, A. Pines, Ultra-low-field NMR relaxation and diffusion measurements using an optical magnetometer, Angew. Chem. Int. Edit. 53 (2014) 9766–9770.
[9] R. Jiménez-Martínez, D.J. Kennedy, M. Rosenbluh, E.A. Donley, S. Knappe, S.J. Seltzer, H.L. Ring, V.S. Bajaj, J. Kitching, Optical hyperpolarization and NMR detection of ^{129}Xe on a microfluidic chip, Nat. Commun. 5 (2014) 3908.
[10] G. Liu, X. Li, X. Sun, J. Feng, C. Ye, X. Zhou, Ultralow field NMR spectrometer with an atomic magnetometer near room temperature, J. Magn. Reson. 237 (2013) 158–163.
[11] T. Oida, M. Tsuchida, T. Kobayashi, Direct detection of magnetic resonance signals in ultra-low field MRI using optically pumped atomic magnetometer with ferrite shields: magnetic field analysis and simulation studies, IEEE Trans. Magn. 48 (2012) 2877–2880.
[12] I.M. Savukov, M.V. Romalis, NMR detection with an atomic magnetometer, Phys. Rev. Lett. 94 (2005) 123001.
[13] I.M. Savukov, S.J. Seltzer, M.V. Romalis, Detection of NMR signals with a radio-frequency atomic magnetometer, J. Magn. Reson. 185 (2007) 214–220.
[14] I. Savukov, T. Karaulanov, Magnetic-resonance imaging of the human brain with an atomic magnetometer, Appl. Phys. Lett. 103 (2013) 043703.
[15] S. Xu, V.V. Yashchuk, M.H. Donaldson, S.M. Rochester, D. Budker, A. Pines, Magnetic resonance imaging with an optical atomic magnetometer, P. Natl. Acad. Sci. USA 103 (2006) 12668–12671.
[16] S. Xu, C. Crawford, S. Rochester, V. Yashchuk, D. Budker, A. Pines, Submillimeter-resolution magnetic resonance imaging at the earth's magnetic field with an atomic magnetometer, Phys. Rev. A 78 (2008) 013404.
[17] M.C.D. Tayler, T. Theis, T.F. Sjolander, J.W. Blanchard, A. Kentner, S. Pustelny, A. Pines, D. Budker, Invited review article: instrumentation for nuclear magnetic resonance in zero and ultralow magnetic field, Rev. Sci. Instrum. 88 (2017) 091101.
[18] S.-m. Hwang, K. Kim, C.S. Kang, S.-J. Lee, Y.-H. Lee, Effective cancellation of residual magnetic interference induced from a shielded environment for precision magnetic measurements, Appl. Phys. Lett. 99 (2011) 132506.
[19] J.O. Nieminen, P.T. Vesanen, K.C.J. Zevenhoven, J. Dabek, J. Hassel, J. Luomahaara, J.S. Penttilä, R.J. Ilmoniemi, Avoiding eddy-current problems in ultra-low-field mri with self-shielded polarizing coils, J. Magn. Reson. 212 (2011) 154–160.
[20] A.W. Overhauser, Polarization of nuclei in metals, Phys. Rev. 92 (1953) 411–415.
[21] I.I. Nicholson, D.J. Lurie, F.J.L. Robb, The application of proton-electron double-resonance imaging techniques to proton mobility studies, J. Magn. Reson. Ser. B 104 (1994) 250–255.
[22] D. Guiberteau, D. Grucker, EPR spectroscopy by dynamic nuclear polarization in low magnetic field, J. Magn. Reson. Ser. B 110 (1996) 47–54.
[23] M.D. Lingwood, T.A. Siaw, N. Sailasuta, B.D. Ross, P. Bhattacharya, S. Han, Continuous flow Overhauser dynamic nuclear polarization of water in the fringe field of a clinical magnetic resonance imaging system for authentic image contrast, J. Magn. Reson. 205 (2010) 247–254.
[24] M.D. Lingwood, I.A. Ivanov, A.R. Cote, S. Han, Heisenberg spin exchange effects of nitroxide radicals on Overhauser dynamic nuclear polarization in the low field limit at 1.5 mT, J. Magn. Reson. 204 (2010) 56–63.
[25] V.S. Zotev, T. Owens, A.N. Matlashov, I.M. Savukov, J.J. Gomez, M.A. Espy, Microtesla MRI with dynamic nuclear polarization, J. Magn. Reson. 207 (2010) 78–88.
[26] S.-J. Lee, K. Kim, C.S. Kang, S.-m. Hwang, Y.-H. Lee, Pre-polarization enhancement by dynamic nuclear polarization in SQUID-based ultra-low-field nuclear magnetic resonance, Supercond. Sci. Tech. 23 (2010) 115008.
[27] S.-J. Lee, J.H. Shim, K. Kim, K.-K. Yu, S.-m. Hwang, Dynamic nuclear polarization in the hyperfine-field-dominant region, J. Magn. Reson. 255 (2015) 114–121.
[28] S.-J. Lee, J.H. Shim, K. Kim, K.-K. Yu, S.-m. Hwang, Magnetic resonance imaging without field cycling at less than earth's magnetic field, Appl. Phys. Lett. 106 (2015) 103702.
[29] M. Ledbetter, I. Savukov, V. Acosta, D. Budker, M. Romalis, Spin-exchange-relaxation-free magnetometry with cs vapor, Phys. Rev. A 77 (3) (2008) 033408.
[30] A. Gusarov, D. Levron, A.B.A. Baranga, E. Paperno, R. Shuker, An all-optical scalar and vector spin-exchange relaxation-free magnetometer employing on–off pump modulation, J. Appl. Phys. 109 (2011) 07E507.